J. Fluid Mech. (2010), *vol.* 658, *pp.* 211–228. © Cambridge University Press 2010
doi:10.1017/S0022112010001667

Oscillatory pipe flows of a yield-stress fluid

YONG SUNG PARK[1]† AND PHILIP L.-F. LIU[1,2]

[1]School of Civil and Environmental Engineering, Cornell University, Ithaca, NY 14853, USA
[2]Institute of Hydrological and Oceanic Sciences, National Central University, Jhongli,
Taoyuan 320, Taiwan

(Received 27 January 2010; revised 30 March 2010; accepted 2 April 2010;
first published online 10 June 2010)

Oscillatory pipe flows of aqueous Carbopol solutions are investigated both experimentally and analytically. Using the PIV technique, the velocity profiles are measured and compared with the numerical solutions based on an elasto-viscoplastic rheological model, in which an elastic spring is serially connected to a regularized Bingham viscoplastic model. The rheological parameters, such as shear modulus of elasticity, yield stress and viscosity, are estimated from steady-shear measurements. Good agreement between the experiments and the model results is observed. It is apparent that the elasticity plays an important role in the unsteady flows of the soft yield-stress fluid studied herein.

Key words: coastal engineering, plastic materials, viscoelasticity

1. Introduction

A muddy seabed can cause significant wave attenuation (Gade 1958; Minirani & Kurup 2007). Better understanding of dynamic responses of mud to wave loadings is a necessity for improving fundamental scientific knowledge and developing practical guidelines for engineering applications. However, rheological properties of muddy seabeds appear to be complex, and depend on the physical and chemical composition of the constituent materials, the concentration and the sea state (see e.g. McAnally *et al.* 2007*a*,*b*).

At one end of the mud rheology spectrum is the elastic solid owing to the internal microscopic structure, while at the other end is the viscous fluid mud with much higher viscosity than that of water (Gade 1958). Naturally, researchers have applied different models to different situations, namely elastic (e.g. Foda 1989; Wen & Liu 1995), viscous (e.g. Gade 1958; Dalrymple & Liu 1978; Liu & Chan 2007; Park, Liu & Clark 2008), viscoelastic (e.g. MacPherson 1980; Jain & Mehta 2009; Mei *et al.* 2010) or viscoplastic (e.g. Mei & Liu 1987; Chan & Liu 2009), to name a few.

However, recent advancements in rheology (e.g. Piau 2007; Cheddadi *et al.* 2008; Luu & Forterre 2009; Putz & Burghelea 2009) suggest that the aforementioned rheological models may be studied in a unified framework. In particular, Luu & Forterre (2009) carried out impact experiments of yield-stress fluids and successfully reproduced important features using an elasto-viscoplastic model, in which an elastic spring is serially connected to a typical viscoplastic model. Other simpler models listed above can be considered as subsets of the elasto-viscoplastic model. Note that

---

† Email address for correspondence: yp54@cornell.edu

a tensorial and three-dimensional generalization of such a model has been already laid out by Saramito (2007, 2009).

One of the objectives of the paper is to provide further experimental evidence of the elasto-viscoplasticity by measuring and calculating the velocity field for oscillatory pipe flows of a yield-stress fluid. Mei & Liu (1987) and more recently Chan & Liu (2009) investigated the response of a Bingham mud to unsteady pressure gradients, which are induced by surface water waves. Chan & Liu (2009) showed that alternating layers of a solid-like plug flow region and fluid-like shear flow region are possible within a Bingham muddy seabed. While considering Stokes' second problem of a yield-stress fluid described by the Herschel–Bulkley model, Balmforth, Forterre & Pouliquen (2009) also predicted the presence of the alternating layers of plug flow and viscous shear flow. However, their experiments, using a kaolin slurry in a partially filled oscillating rectangular box, displayed very different characteristics from those of numerical results. Balmforth *et al.* (2009) speculated that the thixotropy may be responsible for the discrepancy. While the present study has been motivated by the recent theoretical investigations on a viscoplastic muddy seabed (e.g. Chan & Liu 2009), we chose an aqueous Carbopol solution as a surrogate mud. Specifically, the Carbopol solution is known to have a yield stress, without significant thixotropy (Piau 2007) as opposed to natural mud. Moreover, it is optically clear so that quantitative flow visualization technique, e.g. particle image velocimetry (PIV), can be readily employed. More complex behaviours of thixotropic mud are left as future study.

Individual particles of Carbopol take the form of spherical blobs that tend to swell in water and they squeeze each other with increasing concentration (Coussot *et al.* 2009). Thus, small deformations of the material can be recovered elastically. Under large enough shear stress, however, the squeezed blobs can jump from one location to another. Hence, the aqueous Carbopol solution appears to have a yield stress (Piau 2007). Note that the structure causing the macroscopic elastic behaviour still remains while the material flows. Once the applied stress is removed, the repulsive forces of the blobs quickly restore the overall structure, and there is no inherent mechanism responsible for siginificant thixotropy. Note that this property is common to other yield-stress fluids that are formed by microscopic repulsive forces (Coussot *et al.* 2009). On the other hand, materials formed by the attractive interactions, such as clay suspensions, could exhibit substantial hysteresis (Balmforth & Craster 2001).

In the next section (§ 2), the constitutive equations for the Carbopol solution are first reviewed. Then a mathematical model for the pipe flows is formulated and solved numerically in § 3. In § 4 the U-tube experimental setup is described for oscillatory pipe flows. To validate the accuracy of the apparatus and the measuring technique, experiments using sugar water are performed first. Excellent agreement between experimental data and analytical solutions is achieved. Experiments are then carried out with Carbopol solutions. In § 5 experimental data are compared with the numerical simulations for both regularized Bingham flow model and the newly proposed elasto-viscoplastic model. It is clear that the elasticity plays an important role in oscillatory flows of the soft yield-stress fluid. Finally, concluding remarks are presented in § 6.

2. Constitutive relations

The constitutive model employed in this paper can be described as the serial combination of an elastic spring and the Bingham viscoplastic element. After reviewing the constitutive equations, measured values of the rheological parameters

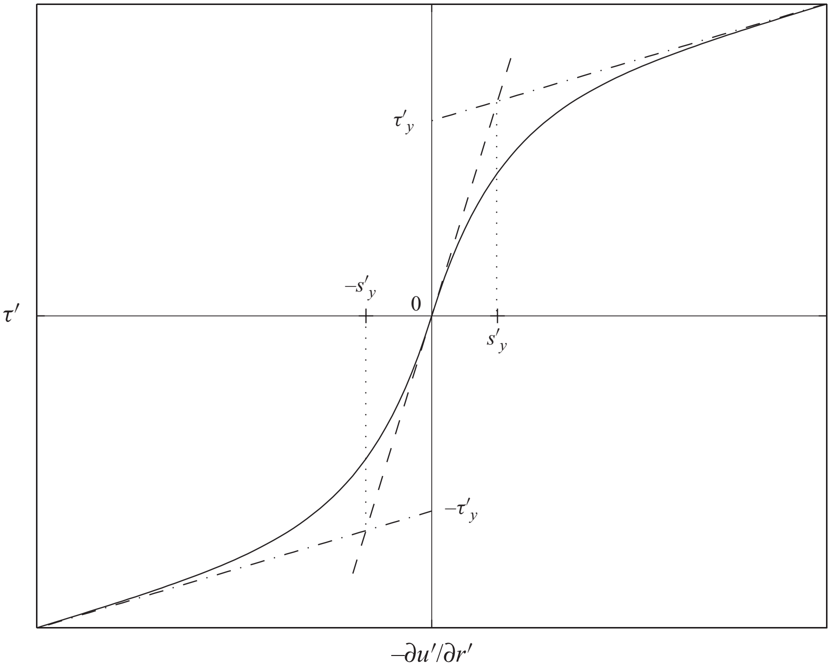

FIGURE 1. Steady constitutive relations for yield-stress fluids: —·—, the Bingham model (2.2); ——, the Papanastasiou model (2.3); – – – – –, the initial Newtonian state (2.4).

(shear modulus of elasticity, yield stress and viscosity) for an aqueous Carbopol solution are reported herein.

2.1. *The Bingham model and its regularized variation*

In a simple pipe flow, the Bingham model in terms of the cylindrical coordinate reads as follows (see figure 1):

$$\frac{\partial u'}{\partial r'} = 0, \qquad |\tau'| \leqslant \tau'_y, \tag{2.1}$$

$$\tau' = -\left(\mu' + \frac{\tau'_y}{|\partial u'/\partial r'|}\right)\frac{\partial u'}{\partial r'}, \qquad |\tau'| \geqslant \tau'_y, \tag{2.2}$$

in which $u'(r', t')$ is the axial velocity, r' is the radial coordinate, t' is the time coordinate, μ' is the dynamic viscosity of the fluid, τ' is the shear stress and τ'_y is the yield stress. This constitutive model has been extensively used in many applications. Analytical solutions are available for simple flows (see Bird, Dai & Yarusso 1983). However, it is often difficult to track the yield surface and the solutions can exhibit singularities in more complex flows, especially when the rate of shear strain vanishes (Balmforth & Craster 2001).

To avoid difficulties arising from the discontinuity in the constitutive relation, Papanastasiou (1987) suggested a regularized version of the Bingham model (see figure 1):

$$\tau' = -\left\{\mu' + \frac{\tau'_y}{|\partial u'/\partial r'|}\left[1 - \exp\left(-\frac{1}{s'_y}\left|\frac{\partial u'}{\partial r'}\right|\right)\right]\right\}\frac{\partial u'}{\partial r'}, \tag{2.3}$$

where s_y' is the characteristic rate of shear strain at which the flow 'yields', as depicted in figure 1. As the rate of shear strain increases (2.3) converges to (2.2), whereas with a vanishing rate of shear strain the model approximates a highly viscous Newtonian fluid, i.e.

$$\tau' \rightarrow -\left(\mu' + \frac{\tau_y'}{s_y'}\right)\frac{\partial u'}{\partial r'}, \quad \frac{\partial u'}{\partial r'} \rightarrow 0. \tag{2.4}$$

That is to say, the regularized model (2.3) is no longer singular even when the rate of shear strain becomes zero, while it can be arbitrarily close to the Bingham model (2.1) and (2.2) with a sufficiently small value of s_y'. Furthermore, this model has been widely utilized for numerical simulations of yield-stress-fluid flows and is known to be computationally economic and robust compared with other kinds of regularized models such as the bi-viscosity model (see e.g. Fan, Phan-Thien & Tanner 2001). Finally, the yield surface can be readily tracked if appropriately defined, for example, as $\partial u'/\partial r' = \pm s_y'$.

2.2. *An elasto-viscoplastic extension of the regularized Bingham model*

The elasto-viscoplastic model based on the regularized Bingham model (2.3) can be written as follows:

$$\frac{\mu_e'}{G'}\frac{\partial \tau'}{\partial t'} + \tau' = -\mu_e'\frac{\partial u'}{\partial r'}, \tag{2.5}$$

in which G' denotes the shear modulus of elasticity of the spring element and

$$\mu_e' = \mu' + \frac{\tau_y'}{|\partial u'/\partial r'|}\left[1 - \exp\left(-\frac{1}{s_y'}\left|\frac{\partial u'}{\partial r'}\right|\right)\right]. \tag{2.6}$$

Note that this model implies that the material behaves like an elastic solid before yielding, while it becomes a linearized Maxwell viscoelastic fluid with a relaxation time $\lambda' = \mu'/G'$ otherwise (Cheddadi *et al.* 2008). We also remark here that the model (2.5) represents one of the simplest ways to add elasticity in the Bingham model and it cannot reproduce nonlinear effects such as normal stress differences (Tanner & Walters 1998). By replacing the time derivative in (2.5) with an appropriate derivative that admits finite deformation (Joseph 1990), one may recover a more general nonlinear model, as suggested by Saramito (2007).

2.3. *Rheological measurements of the aqueous Carbopol solution*

For the present experiments, Carbopol 940 polymer (Lubrizol Advanced Materials, Inc.) with 0.075 % concentration by weight was prepared and neutralized with sodium hydroxide. Rheological properties of the Carbopol solution were measured using a rheometer (Anton-Paar Physica MCR 300) with a cone geometry (CP25-4.5sn478) and a plate. The flow curve shown in figure 2 was obtained by measuring the rate of shear strain while varying the shear stress every one second. To estimate hysteretic effects, the shear stress was first gradually increased to 5 Pa, then decreased to −5 Pa, and finally increased again to zero. Some hysteresis is seen, especially when the flow field within the gap decelerates near $\tau' = \pm 5$ Pa. The parameters for the regularized Bingham model (2.3) are then found by least-squares curve fitting across the entire data with the R-square value being 0.98, and are summarized in table 1, in which γ is the specific gravity of the material. We remark that the model parameters can differ widely depending on the range of data used for the curve fitting (Putz & Burghelea 2009). As shown in the inset of figure 2, the regularized Bingham model (2.3) shows discrepancy with the measured data for low rate of shear strain. Indeed,

G' (Pa)	τ'_y (Pa)	μ' (Pa s)	s'_y (s^{-1})	γ
5.6	2.4	2.2×10^{-1}	5.7×10^{-2}	1.05

TABLE 1. Rheological parameters for the 0.075 % Carbopol solution.

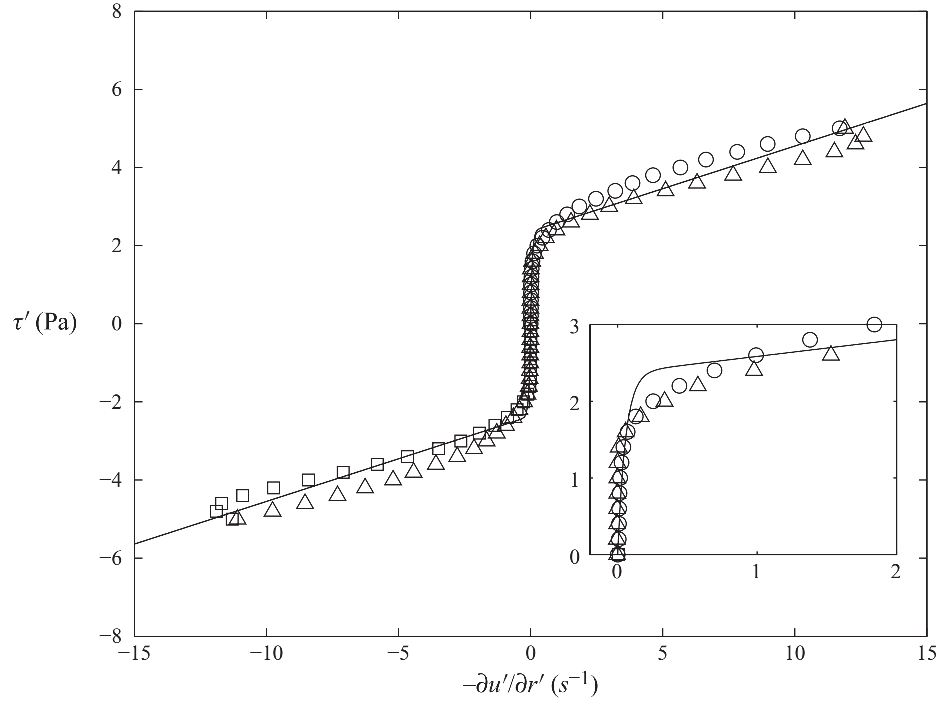

FIGURE 2. Steady rheological measurements of the 0.075 % Carbopol solution: ○, from zero shear stress to 5 Pa; △, from 5 Pa to −5 Pa; □, from −5 Pa to 0; ——, the fitted regularized Bingham model (2.3). The inset is a close-up of low rate of shear strain region.

the Herschel–Bulkley model could fit the data better in this range of the rate of shear strain (e.g. Piau 2007). Since the focus of the present study is to explore the elastic effect of the material, we chose to use the Bingham model for its relative simplicity in the numerical calculation presented herein.

The dependence of the shear strain on the applied shear stress is shown in figure 3, in which the shear strain is obtained as the time integral of the rate of shear strain shown in figure 2 and X' denotes the particle displacement in the axial direction. As we are interested in the solid regime with small shear strains, the data are plotted in the log–log scale in this figure. The transition from the solid regime to the fluid regime is seen as the gradual change in the slope of the curve (Putz & Burghelea 2009). After fitting the data with a smoothing spline (smoothing parameter $p = 0.99994$) in the linear scale, the shear modulus of elasticity is obtained as the slope at the zero shear stress, which is 5.6 Pa (see table 1). While this procedure provides the shear modulus at zero strain and at zero frequency, as desired, oscillatory tests have also been carried out with different frequency (2–4 Hz) and strain amplitude (0.5–10 %)

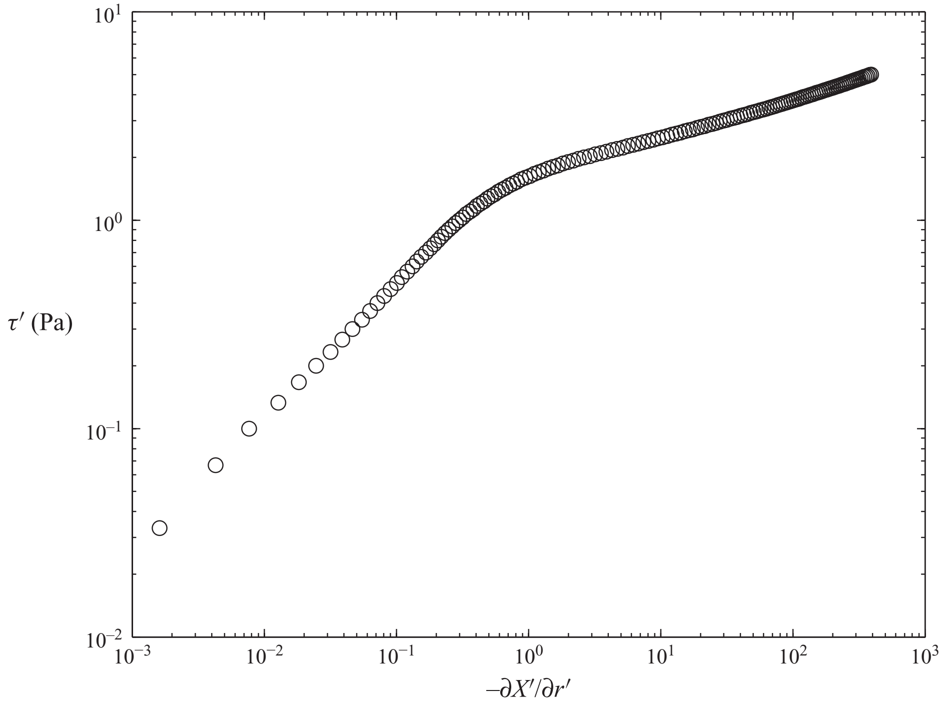

FIGURE 3. Stress–strain curve of the 0.075 % Carbopol solution with shear stress increasing from zero to 5 Pa.

for independent comparison. The storage modulus was measured to be between 3 and 10 Pa, which is within the same order of magnitude with the shear modulus estimated from the steady-shear measurements.

3. Theoretical formulation

3.1. *The governing equation*

The governing equation for uni-directional flows in a circular pipe can be written in dimensional form as

$$\frac{\partial u'}{\partial t'} = -\frac{1}{\rho'}\frac{\partial p'}{\partial x'} - \frac{1}{\rho' r'}\frac{\partial}{\partial r'}(r'\tau'), \tag{3.1}$$

in which x' is the axial coordinate, ρ' is the density of the fluid and p' is the pressure. Initially, both the velocity and the shear stress are zero everywhere. The flow is driven by the pressure gradient and the no-slip condition is applied on the pipe wall.

Denoting

$$-\frac{1}{\rho'}\frac{\partial p'}{\partial x'} = P' f(\omega' t'), \tag{3.2}$$

where f is a non-dimensionalized oscillatory function with ω' being its frequency, the following dimensionless variables are introduced:

$$u = \frac{u'}{P'/\omega'}, \quad r = \frac{r'}{R'}, \quad t = \omega' t', \quad \tau = \frac{\tau'}{G'}. \tag{3.3}$$

where R' is the inner radius of the pipe. We use the shear modulus of elasticity G' as the characteristic stress, expecting the important role of the elasticity in transient flows as suggested by Cheddadi *et al.* (2008). The governing equation (3.1) and the constitutive relation (2.6) and (2.5) can be expressed in terms of the dimensionless variables as follows:

$$\frac{\partial u}{\partial t} = f(t) - \frac{1}{Re\,We}\frac{1}{r}\frac{\partial}{\partial r}(r\tau), \tag{3.4}$$

$$De\,h\,\frac{\partial \tau}{\partial t} + \tau = -We\,h\,\frac{\partial u}{\partial r}, \tag{3.5}$$

$$h = 1 + \frac{Bi}{|\partial u/\partial r|}\left[1 - \exp\left(-N\left|\frac{\partial u}{\partial r}\right|\right)\right], \tag{3.6}$$

where the Reynolds (Re), Weissenberg (We), Deborah (De) and Bingham (Bi) numbers and N are defined as

$$Re = \frac{\rho'\omega' R'^2}{\mu'}, \tag{3.7}$$

$$We = \frac{\mu'}{G'}\frac{P'/\omega'}{R'}, \tag{3.8}$$

$$De = \frac{\mu'}{G'}\omega', \tag{3.9}$$

$$Bi = \tau'_y\frac{R'}{\mu'(P'/\omega')}, \tag{3.10}$$

$$N = \frac{P'/\omega'}{s'_y R'}, \tag{3.11}$$

respectively. We remark that the regularized Bingham model (2.3) is recovered by dropping the time-derivative term in (3.5), and the dimensionless momentum equation, (3.4), reduces to

$$\frac{\partial u}{\partial t} = f(t) - \frac{1}{Re}\frac{1}{r}\frac{\partial}{\partial r}\left(r\,h\,\frac{\partial u}{\partial r}\right), \tag{3.12}$$

where h is given by (3.6).

3.2. *Numerical simulations*

To solve the system of equations (3.4)–(3.6), an iterative scheme was employed in which the nonlinear viscosity h is calculated based on the result from the previous iteration at each time step, while the linear operators are discretized by the implicit scheme similar to that of Manos, Marinakis & Tsangaris (2006). In view of (2.4), $h = 1 + Bi\,N$ is used as an initial guess at each time step. The iteration continues until the maximum relative error between the respective results from the current and the previous iterations becomes smaller than 10^{-6}. With the parameters representing the experimental conditions, numerical solutions converge quickly within five iterations. Also, numerical solutions reach the periodic state before the third period of the pressure forcing.

4. Experiments

4.1. *Experimental setup*

Figure 4 shows a picture of the U-tube facility designed for the experiments. One end of the U-tube is connected to a mechanically activated pneumatic piston, while

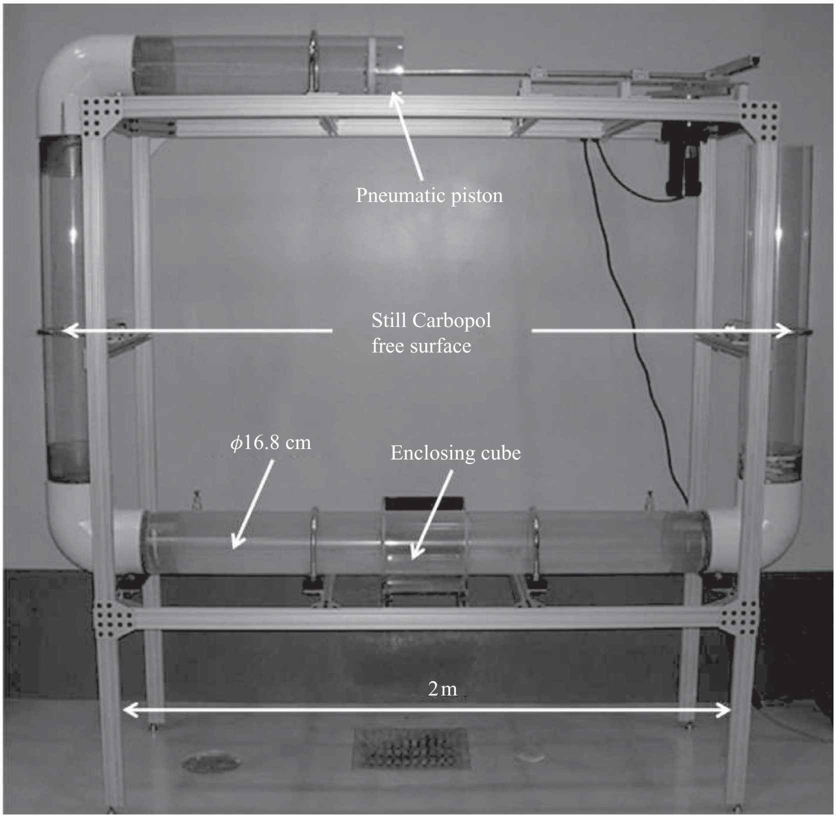

FIGURE 4. The U-tube used for the experiments.

the other end is open to atmosphere. Up to about half of the vertical columns was filled with the Carbopol solution as indicated in the figure. The U-tube is made of acrylic circular pipes with inner diameter $D' = 2R' = 16.8$ cm, which is about four times larger than the Stokes boundary-layer thickness based on the viscosity of the Carbopol solution and the typical frequency of the U-tube experiments. The total length of the horizontal section of the U-tube is $l' = 2$ m. At the mid-section the circular pipe is enclosed by a cube, which is 22 cm long. The cube was filled with water and was used as a prism to minimize the unwelcome refraction during PIV imaging.

With one end open to the air, the natural frequency ω_0' of the U-tube is determined in terms of the horizontal length l' (Park 2009):

$$\omega_0' = \sqrt{\frac{2g'}{l'}}, \tag{4.1}$$

in which g' denotes the gravitational acceleration. With $l' = 2$ m, the natural frequency for the system depicted in figure 4 is roughly $\omega_0' \approx 3\ \mathrm{rad\,s^{-1}}$.

Finally, two acoustic wave gauges (Banner Engineering S18U) were installed, one in each vertical column, to measure the free surface elevations simultaneously. The pressure gradient along the U-tube can then be calculated.

4.2. *Velocity field measurements*

The piston was put in sinusoidal motions with $\omega' \approx \omega'_0$. For each experiment data collections were initiated five minutes after the start-up of the piston so that a quasi-steady state had been established in the system. The fluids were seeded with the hollow glass spheres (Potters Industry 110P8) with typical diameter 11 µm and the specific gravity 1.1. The PIV system in the DeFrees Hydraulics Laboratory at Cornell University was employed to resolve velocity fields across the whole diameter of the tube at the rate of 10 Hz for two minutes. The vertical resolution of the PIV data was 0.2 mm. Detailed description about the PIV system and the analysis procedure can be found in Park (2009).

4.3. *Preliminary test with a Newtonian fluid*

To ensure that the experimental set-up and assumptions in the theoretical models are adequate, a set of experiments was first performed using sugar water of 35 % weight concentration ($\rho' = 1156$ kg m^{-3}, $\mu' = 9.1 \times 10^{-3}$ Pa s).

With the sinusoidal pressure-gradient loading $f(t) = \mathrm{e}^{\mathrm{i}t}$ and the constant viscosity $h = 1$, the analytical solution of (3.12) is found as

$$u(r, t) = \mathrm{Re}\left\{\mathrm{i}\mathrm{e}^{\mathrm{i}t}\left(\frac{\mathrm{J}_0(kr)}{\mathrm{J}_0(k)} - 1\right)\right\}, \tag{4.2}$$

in which Re( ) means the real part of the complex-valued expression, J_0 is the Bessel function of the first kind of zeroth order and k is given as

$$k^2 = -\mathrm{i}Re. \tag{4.3}$$

The radial profiles of dimensionless axial velocity at four different phases for the case with $P' = 0.167$ m s^{-2} and $\omega' = 2.927$ rad s^{-1} are shown in figure 5. In the figure, a stretched radial coordinate

$$\eta = \frac{R' - r'}{\sqrt{\pi}\delta'} \tag{4.4}$$

has been used in which the Stokes boundary-layer thickness of the fluid is written as

$$\delta' = \sqrt{\frac{2\nu'}{\omega'}}, \tag{4.5}$$

where $\nu' = \mu'/\rho'$ is the kinematic viscosity. Note that only the region near the wall ($0 \leqslant \eta \leqslant 5$) is presented in the figure. Very good agreement between the measured data and the analytical solution (4.2) is observed. The flow reversal is accurately captured by the PIV measurement. During the experiments, no significant vibration of the system was detected and the flow was axisymmetric and axially uniform within the field-of-view of the PIV data.

4.4. *Experiments with the Carbopol solution*

Four experimental cases were performed by changing the amplitude and the frequency of the pneumatic piston of the U-tube, which are summarized in table 2. The corresponding values of the dimensionless parameters are also shown in the table. By visual observation, flows in the present experiments appear to be laminar, consistent with the small Reynolds numbers.

Case no.	P' (m s^{-2})	ω' (rad s^{-1})	Re	We	De	Bi	N
Y1	0.103	3.786	128.5502	0.0126	0.1475	33.4656	5.7050
Y2	0.191	3.109	105.5633	0.0285	0.1211	14.8198	12.8829
Y3	0.304	3.364	114.2216	0.0419	0.1311	10.0748	18.9504
Y4	0.467	2.994	101.6586	0.0724	0.1167	5.8370	32.7090

TABLE 2. Experimental cases.

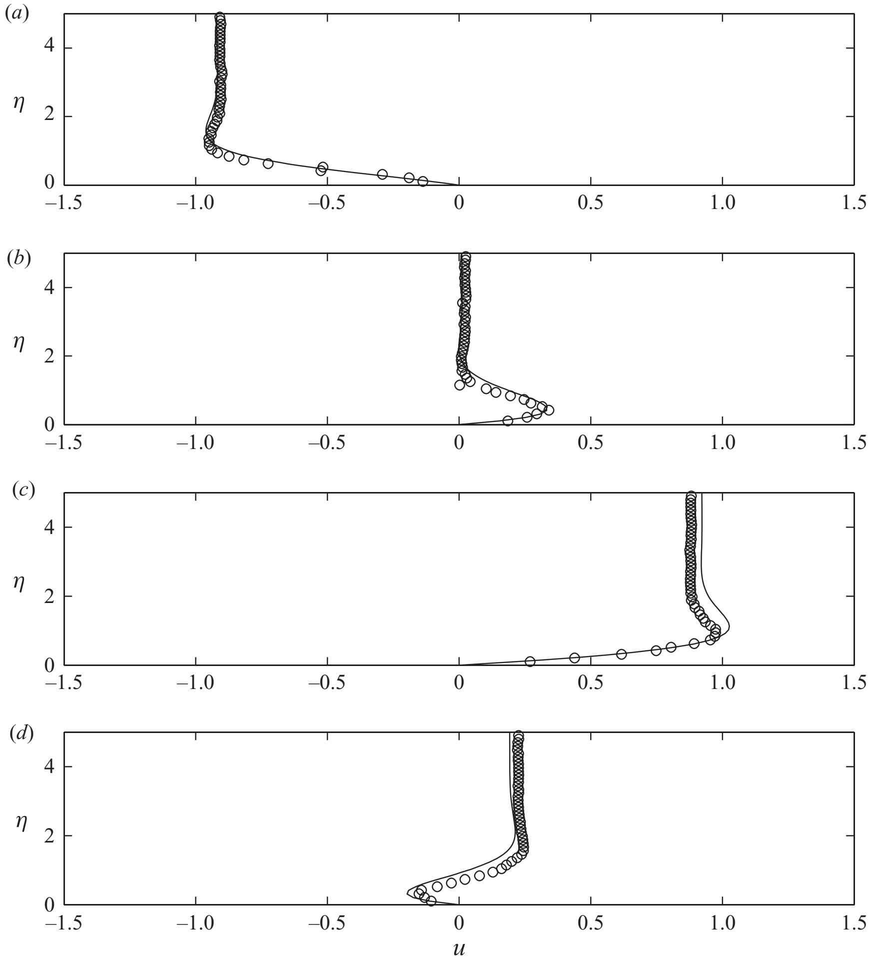

FIGURE 5. Radial profiles of the dimensionless axial velocity for the sugar water experiments at four different phases during the 11th period: ○, PIV data; ——, the analytical solution (4.2). (*a*) $t/2\pi = 10.32$, (*b*) $t/2\pi = 10.50$, (*c*) $t/2\pi = 10.69$ and (*d*) $t/2\pi = 10.97$.

5. Experimental data and numerical results

5.1. *Data–model comparison with numerical results using the regularized Bingham model*

In this section, we first show the comparison between experimental data for the velocity field and those of numerical solution using the regularized Bingham model

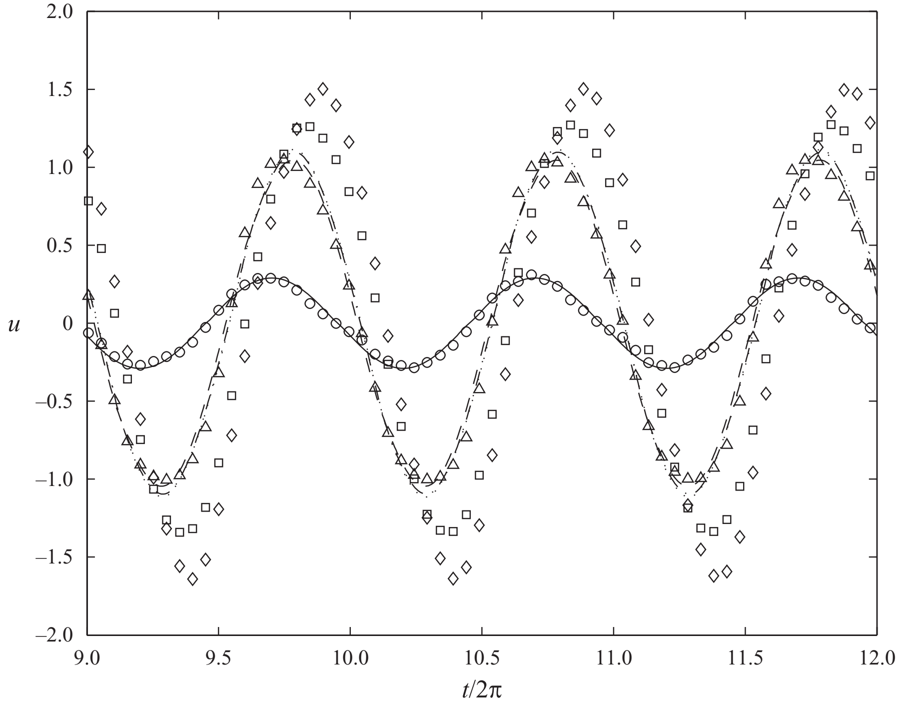

FIGURE 6. Time histories of the dimensionless axial velocity at four different radial positions for the case Y2: ○, PIV data at $r = 0.96$; △, PIV data at $r = 0.62$; □, PIV data at $r = 0.31$; ◇, PIV data at $r = 0$; ——, the numerical solution using the regularized Bingham model (2.3) at $r = 0.96$; – – – – –, the numerical solution at $r = 0.62$; — · —, the numerical solution at $r = 0.31$; · · · · ·, the numerical solution at $r = 0$.

(2.3). Only the comparisons for case Y2 are shown, which are similar to other cases. In figures 6 and 7, time histories of the velocity at different radial locations and the snapshots of the velocity profiles are shown, respectively. Also plotted in figure 7 is the analytical solution for a Newtonian fluid with the same viscosity as that of the Carbopol solution ($\mu' = 0.2182$ Pa s).

Evolution of unyielded plug flow and sheared viscous flow has been considered the key feature of unsteady Bingham fluid flows, as pointed out by Balmforth *et al.* (2009) and Chan & Liu (2009). Because of the zero-shear-stress condition imposed along the centreline of the pipe, the numerical solution, based on the Bingham flow model, shows the plug flow near the centre of the pipe at all times. More interestingly, two disconnected plug flow regions are observed in the numerical solution when the centreline velocity decelerates. One of these plug flow regions is near the centreline and the other is close to the wall as shown in figure 7(*b*), which is consistent with the semi-analytical solution of Chan & Liu (2009).

As expected, the agreement between experimental data and numerical solutions is poor. Indeed, the effect of elasticity under unsteady motion of the yield-stress fluid is manifested by the substantial overshooting in the centreline velocity. Since the material is strictly rigid in the solid regime according to the traditional Bingham model, the overshooting cannot be captured. Note that, despite the complex behaviour of the Carbopol solution, the measured data clearly show periodicity (see figure 6).

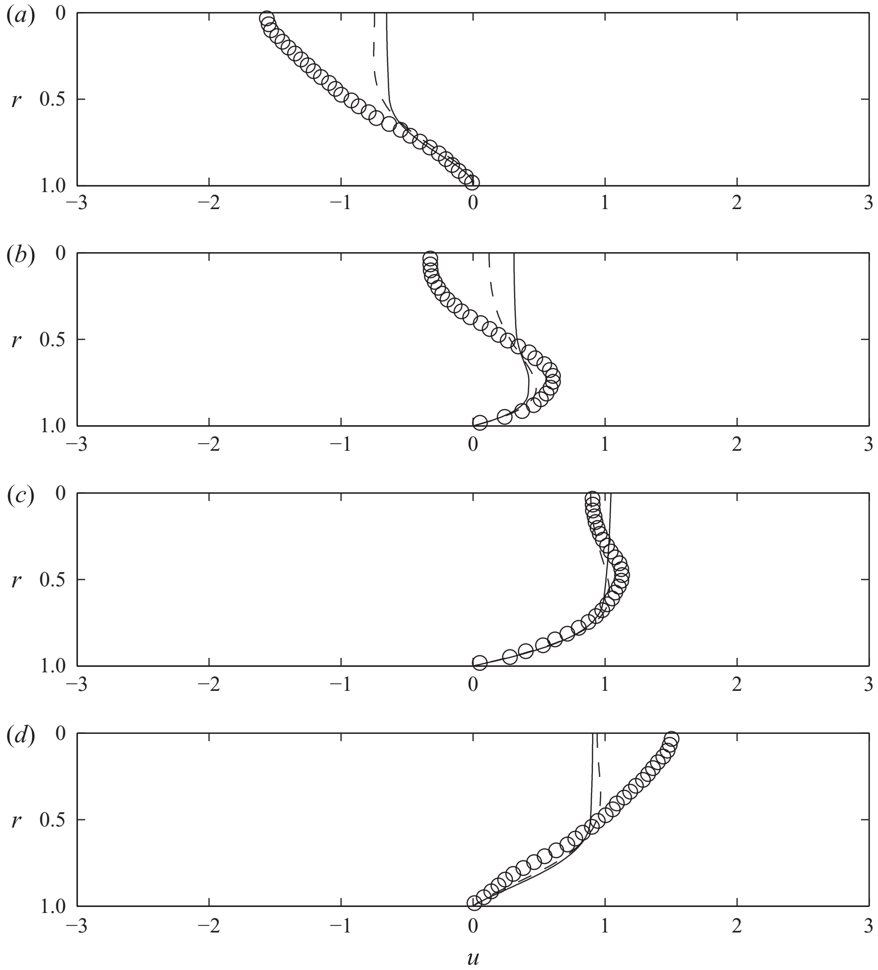

FIGURE 7. Radial profiles of the dimensionless axial velocity for the case Y2 at four different phases during the 11th period: ○, PIV data; ——, the numerical solution using the regularized Bingham model (2.3); – – – – –, the analytical solution for a Newtonian fluid with the same viscosity as that of the Carbopol solution. (*a*) $t/2\pi = 10.44$, (*b*) $t/2\pi = 10.59$, (*c*) $t/2\pi = 10.74$ and (*d*) $t/2\pi = 10.89$.

5.2. *Data–model comparison with numerical results using the elasto-viscoplastic constitutive relation*

The substantial overshooting shown in figure 7 cannot be fully explained by the viscous effects alone. On the other hand, if the elasticity is included, the overshooting can be accounted for, which is the characteristic of the elasto-viscoplastic model (3.5) and (3.6). The resulting numerical solutions are compared with the experimental data for all four cases in figures 8–11.

Overall, the data–model agreement is much better than those shown in figures 6 and 7 in which the regularized Bingham constitutive relation is used. In particular, the overshooting in the centreline velocities and the ostensible curvatures in the radial profiles are well captured.

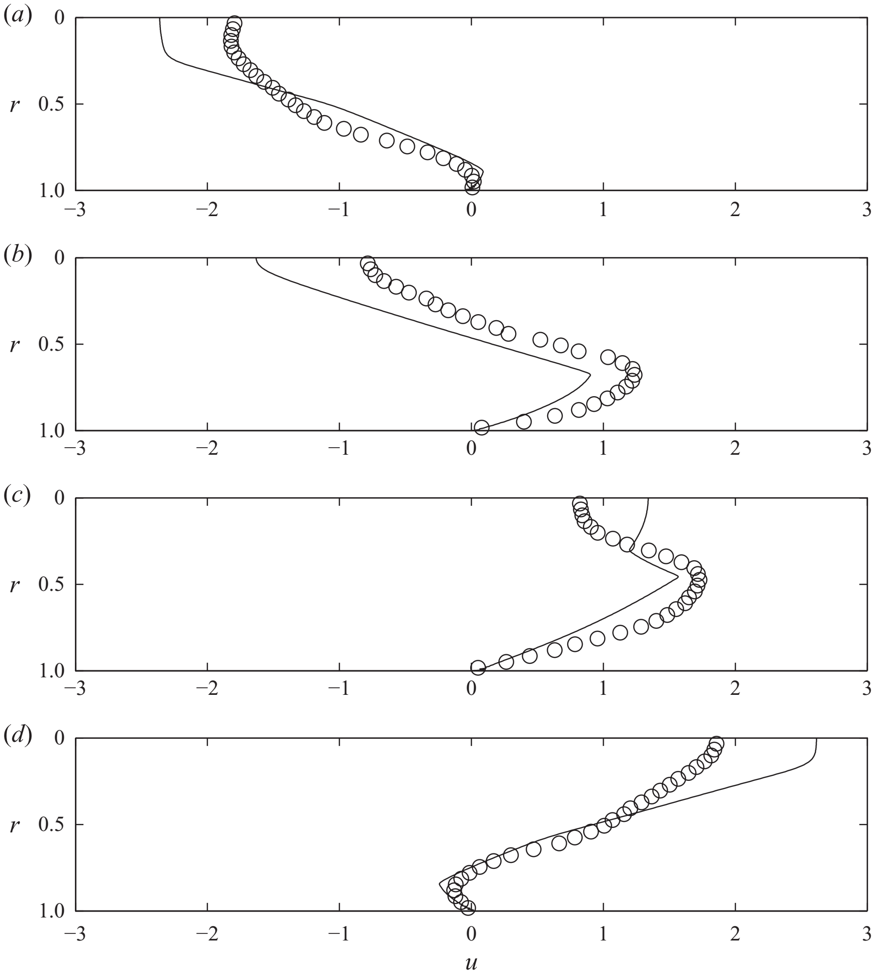

FIGURE 8. Radial profiles of the dimensionless axial velocity for case Y1 at four different phases during the 11th period: ○, PIV data; ——, the numerical solution using the new rheological values. (*a*) $t/2\pi = 10.43$, (*b*) $t/2\pi = 10.61$, (*c*) $t/2\pi = 10.79$ and (*d*) $t/2\pi = 10.97$.

In the numerical results of velocity profiles, sharp corners are observed, indicating the transition from solid to liquid phase. If the viscous part of the rheology strictly follows the Bingham model, a sharp interface (the yield surface) between the purely elastic phase and the linear viscoelastic phase occurs, and the derivatives of the velocity and the shear stress are discontinuous across the yield surface. Even with the regularization, if the spatial or the temporal resolution in the numerical scheme is not high enough to capture the smoothened transition, similar discontinuity would occur in the numerical calculation. Additional simulations with orders-of-magnitude greater values of s'_y indeed showed smooth velocity profiles with no such discontinuities.

The solid–fluid transition during the flow can also be described in terms of the deformation of the material during the flow. Three kinds of strains, i.e. the total strain

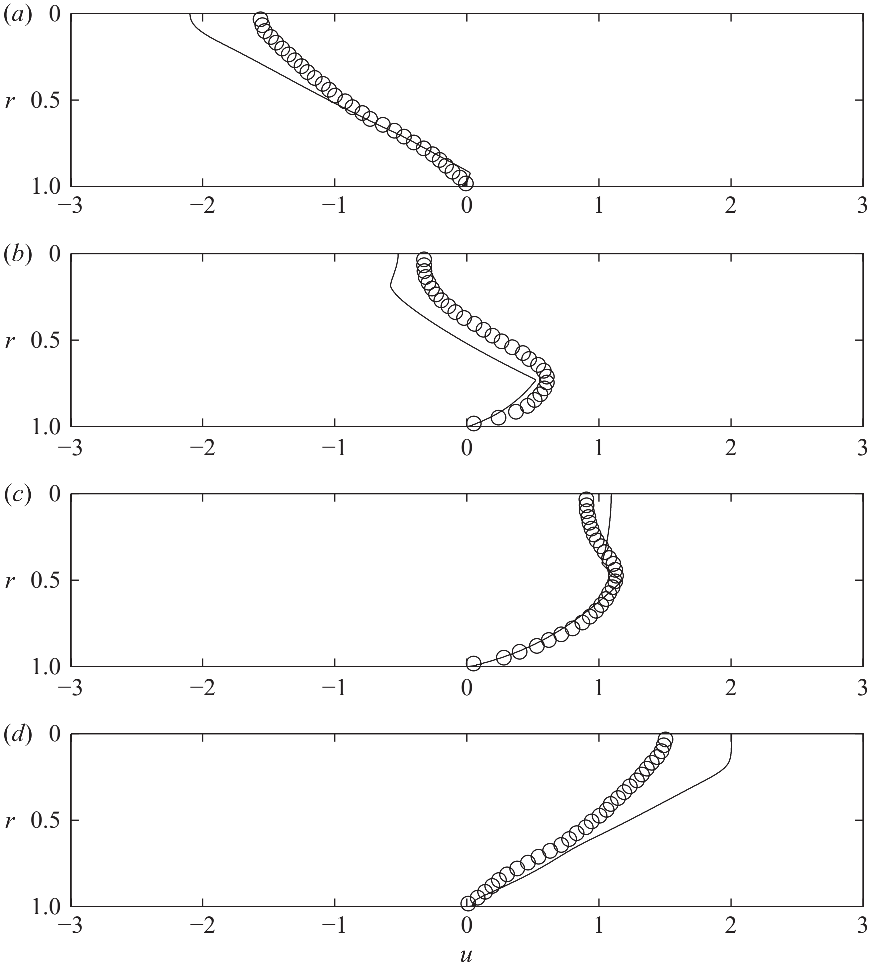

FIGURE 9. Radial profiles of the dimensionless axial velocity for case Y2 at four different phases during the 11th period: ○, PIV data; ——, the numerical solution using the new rheological values. (*a*) $t/2\pi = 10.44$, (*b*) $t/2\pi = 10.59$, (*c*) $t/2\pi = 10.74$ and (*d*) $t/2\pi = 10.89$.

(ϵ_t), the elastic strain (ϵ_e) and the viscous strain (ϵ_v) can be defined as follows:

$$\epsilon_t = \int \frac{\partial u'}{\partial r'} \mathrm{d}t, \tag{5.1}$$

$$\epsilon_e = \tau'/G', \tag{5.2}$$

$$\epsilon_v = \epsilon_t - \epsilon_e. \tag{5.3}$$

For example, time histories of the deformation at two different radial positions for the case Y4 are depicted in figure 12. One can clearly see from figure 12(*a*) that the material near the centre of the pipe never yields, while periodic transition of the material state is observed near the wall. Accordingly, the elastic deformation dominates near the centre, while the viscous contribution is more significant near the wall. It is interesting to see that the phase difference between the elastic and the viscous deformations near the wall is close to 90°, as if it were simply viscoelastic.

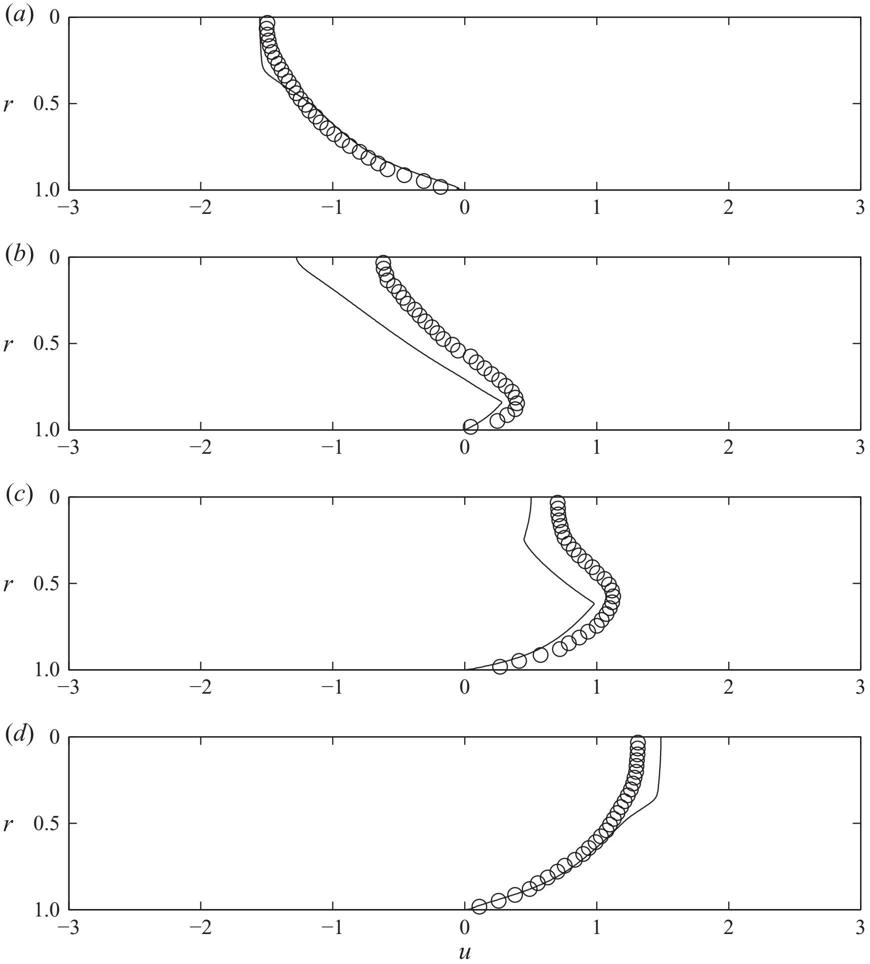

FIGURE 10. Radial profiles of the dimensionless axial velocity for case Y3 at four different phases during the 10th period: ○, PIV data; ——, the numerical solution using the new rheological values. (*a*) $t/2\pi = 10.37$, (*b*) $t/2\pi = 10.53$, (*c*) $t/2\pi = 10.69$ and (*d*) $t/2\pi = 10.85$.

6. Concluding remarks

Motivated by the need to understand the dynamic behaviour of non-Newtonian mud in the coastal environment, oscillatory pipe flows of a yield-stress fluid (an aqueous Carbopol solution being used as the surrogate mud) in the U-tube have been experimentally investigated. Most importantly, we have provided experimental evidence of the significant elastic effects of the material subject to unsteady motion, which is consistent with other recent experiments (e.g. Luu & Forterre 2009). Furthermore, the numerical simulation using a minimal elasto-viscoplastic model with three constant parameters successfully reproduced main features of the experimental results. However, further improvement to the theoretical model would be required to simulate smooth transition from solid to liquid regimes while avoiding excessive overshooting in the centreline velocity.

We remark here that our experimental results may provide a useful framework for the study of cohesive sediments in coastal and fluvial environments, in the sense

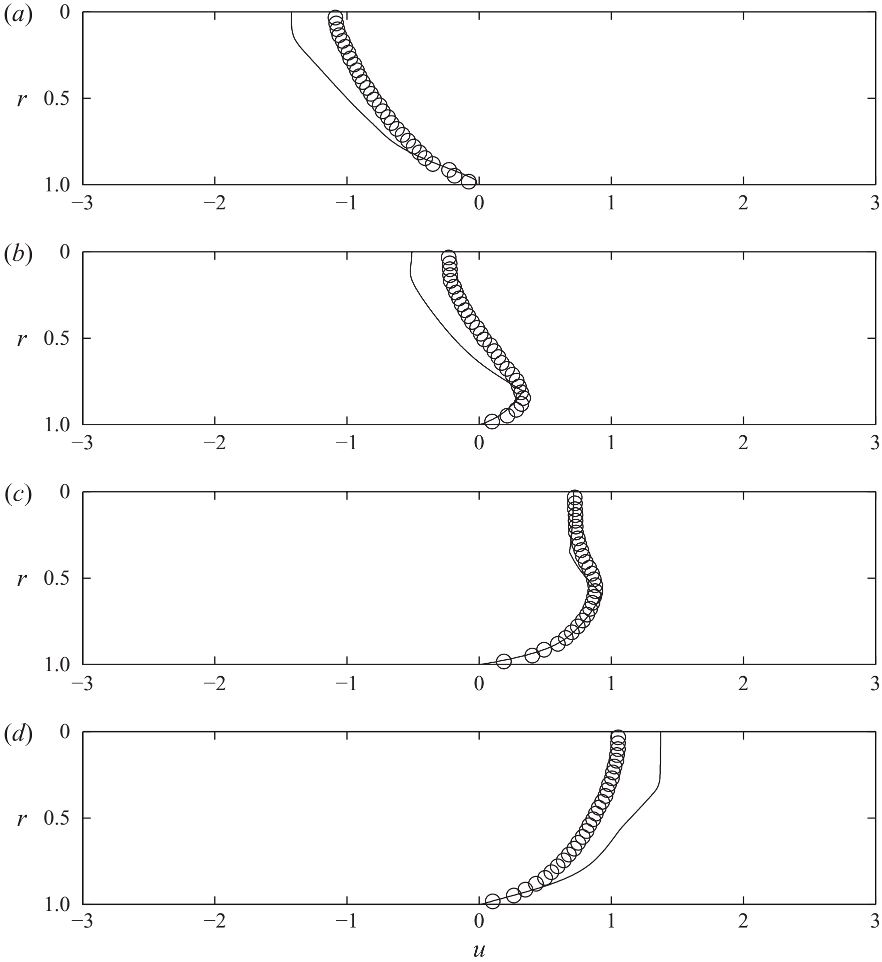

FIGURE 11. Radial profiles of the dimensionless axial velocity for case Y4 at four different phases during the 10th period: ○, PIV data; ——, the numerical solution using the new rheological values. (*a*) $t/2\pi = 10.43$, (*b*) $t/2\pi = 10.57$, (*c*) $t/2\pi = 10.71$ and (*d*) $t/2\pi = 10.86$.

that other simpler models such as viscous, elastic, viscoelastic and viscoplastic are subsets of the elasto-viscoplastic model employed in the present research. Of course, various types of materials need to be examined to extend the results to the real muds.

This work was supported by grants from the National Science Foundation and the Office of Naval Research to Cornell University. P.L.-F.L. would like to acknowledge the support of the Humbolt Foundation through a Research Award during the preparation of the paper. Y.S.P. would also like to acknowledge the support of the Korea Science and Engineering Foundation under grant number M06-2004-000-10541. The authors wish to thank Professor C. Cohen, Professor L. A. Archer and Mr H. Qi for their help in preparation and rheological measurement of the Carbopol

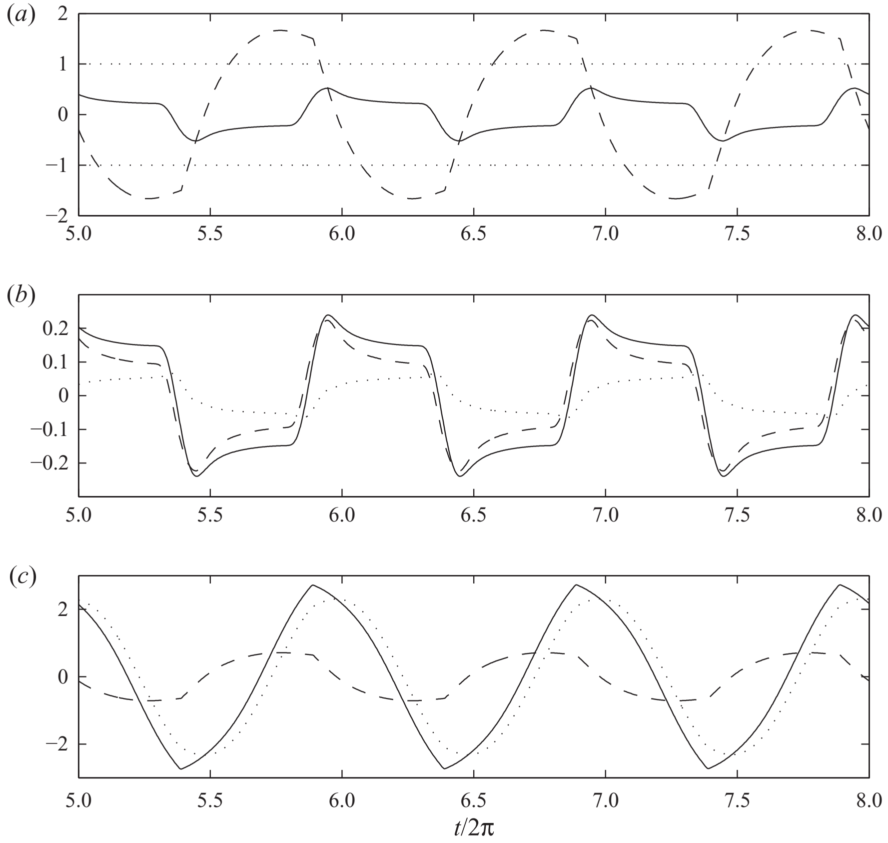

FIGURE 12. Time histories of the strains for the case Y4. (*a*) The elastic strain normalized by the critical strain (τ_y'/G') at two different radial positions: ——, $r = 0.1$; – – – – –, $r = 0.9$; · · · · ·, the solid–fluid transition criteria. (*b*) At $r = 0.1$: ——, ϵ_t; – – – – –, ϵ_e; · · · · ·, ϵ_v. (*c*) At $r = 0.9$: ——, ϵ_t; – – – – –, ϵ_e; · · · · ·, ϵ_v.

solutions. Finally, the authors thank the reviewers, whose suggestions significantly improved the quality of the presentation.

REFERENCES

BALMFORTH, N. J. & CRASTER, R. V. 2001 Geophysical aspects of non-Newtonian fluid mechanics. In *Geomorphological Fluid Mechanics* (ed. P. A. Tyvand & A. Provenzale), pp. 34–51. Springer.

BALMFORTH, N. J., FORTERRE, Y. & POULIQUEN, O. 2009 The viscoplastic Stokes layer. *J. Non-Newton. Fluid Mech.* **158**, 46–53.

BIRD, R. B., DAI, G. C. & YARUSSO, B. J. 1983 The rheology and flow of viscoplastic materials. *Rev. Chem. Engng* **1**, 1–70.

CHAN, I.-C. & LIU, P. L.-F. 2009 Responses of Bingham-plastic muddy seabed to a surface solitary wave. *J. Fluid Mech.* **618**, 155–180.

CHEDDADI, I., SARAMITO, P., RAUFASTE, C., MARMOTTANT, P. & GRANER, F. 2008 Numerical modelling of foam Couette flows. *Eur. Phys. J.* E 27, 123–133.

COUSSOT, P., TOCQUER, L., LANOS, C. & OVARLEZ, G. 2009 Macroscopic vs. local rheology of yield stress fluids. *J. Non-Newton. Fluid Mech.* **158**, 85–90.

Dalrymple, R. A. & Liu, P. L.-F. 1978 Waves over soft muds: a two-layer model. *J. Phys. Oceanogr.* **8**, 1121–1131.

Fan, Y., Phan-Thien, N. & Tanner, R. I. 2001 Tangential flow and advective mixing of viscoplastic fluids between eccentric cylinders. *J. Fluid Mech.* **431**, 65–89.

Foda, M. A. 1989 Sideband damping of water waves over a soft bed. *J. Fluid Mech.* **201**, 189–201.

Gade, H. G. 1958 Effects of a nonrigid, impermeable bottom on plane surface waves in shallow water. *J. Mar. Res.* **16**, 61–82.

Jain, M. & Mehta A. J. 2009 Role of basic rheological models in determination of wave attenuation over muddy seabeds. *Cont. Shelf Res.* **29**, 642–651.

Joseph, D. D. 1990 *Fluid Dynamics of Viscoelastic Liquids*. Springer.

Liu, P. L.-F. & Chan, I.-C. 2007 On long wave propagation over a fluid-mud seabed. *J. Fluid Mech.* **579**, 467–480.

Luu, L.-H. & Forterre, Y. 2004 Drop impact of yield-stress fluids. *J. Fluid Mech.* **632**, 301–327.

MacPherson, H. 1980 The attenuation of water waves over a non-rigid bed. *J. Fluid Mech.* **97**, 721–742.

Mahaut, F., Chateau, X., Coussot, P. & Ovarlez, G. 2008 Yield stress and elastic modulus of suspensions of noncolloidal particles in yield stress fluids. *J. Rheol.* **52**, 287–313.

Manos, T., Marinakis, G. & Tsangaris, S. 2006 Oscillating viscoelastic flow in a curved duct: exact analytical and numerical solution. *J. Non-Newton. Fluid Mech.* **135**, 8–15.

McAnally, W. H., Friedrichs, C., Hamilton, D., Hayter, E., Shrestha, P., Rodriguez, H., Sheremet, A. & Teeter, A. 2007*a* Management of fluid mud in estuaries, bays and lakes. Part 1. Present state of understanding on character and behavior. ASCE Task Committee on Management of Fluid Mud. *J. Hydraul. Engng* **133**, 9–22.

McAnally, W. H., Friedrichs, C., Hamilton, D., Hayter, E., Shrestha, P., Rodriguez, H., Sheremet, A. & Teeter, A. 2007*b* Management of fluid mud in estuaries, bays and lakes. Part 2. Measurement, modeling and management. ASCE Task Committee on Management of Fluid Mud. *J. Hydraul. Engng* **133**, 23–38.

Mei, C. C., Krotov, M., Huang, Z & Aode, H. 2010 Short and long waves over a muddy seabed. *J. Fluid Mech.* **643**, 33–58.

Mei, C. C. & Liu, K.-F. 1987 A Bingham-plastic model for a muddy seabed under long waves. *J. Geophys. Res.* **92**, 14581–14594.

Minirani, S. & Kurup, P. G. 2007 Energy attenuation of sea surface waves through generation of interface waves on viscoelastic bottom as in the mud banks, SW coast of India. *J. Indian Geophys. Union* **11**, 143–146.

Papanastasiou, T. C. 1987 Flows of materials with yield. *J. Rheol.* **31**, 385–404.

Park, Y. S. 2009 Seabed dynamics and breaking waves. PhD dissertation, Cornell University.

Park, Y. S., Liu, P. L.-F. & Clark, S. J. 2008 Viscous flows in a muddy seabed induced by a solitary wave. *J. Fluid Mech.* **598**, 383–392.

Piau, J. M. 2007 Carbopol gels: elastoviscoplastic and slippery glasses made of individual swollen sponges: meso- and macroscopic properties, constitutive equations and scaling laws. *J. Non-Newton. Fluid Mech.* **144**, 1–29.

Putz, A. M. V. & Burghelea, T. I. 2009 The solid–fluid transition in a yield stress shear thinning physical gel. *Rheol. Acta* **48**, 673–689.

Saramito, P. 2007 A new constitutive equation for elastoviscoplastic fluid flows. *J. Non-Newton. Fluid Mech.* **145**, 1–14.

Saramito, P. 2009 A new elastoviscoplastic model based on the Herschel–Bulkley viscoplastic model. *J. Non-Newton. Fluid Mech.* **158**, 154–161.

Tanner, R. I. & Walters, K. 1998 *Rheology: An Historical Perspective*. Elsevier.

Wen, J. & Liu, P. L.-F. 1995 Mass transport in water waves over an elastic bed. *Proc. R. Soc.* A **450**, 371–390.